The International Journal of Advanced Manufacturing Technology (2022) 119:2691–2707
https://doi.org/10.1007/s00170-021-08359-7

ORIGINAL ARTICLE

Surface quality adjustment and controlling mechanism of machined surface layer in two-step milling of titanium alloy

Rufeng Zhang[1,2] · Anhai Li[1,2] · Xuhao Song[1,2]

Received: 25 August 2021 / Accepted: 8 November 2021 / Published online: 4 January 2022

Abstract
In the two-step cutting process, due to the combined effects of mechanical and thermal deformation, the microstructure and residual stress of the workpiece are changed with the change of roughing parameters, which affects the machined surface quality. In this paper, the two-step milling (roughing and then finishing) experiments of Ti-6Al-4V titanium alloy were designed to analyze the effect of different roughing parameters on the cutting force of roughing and finishing, the residual stress of finishing surface, and the microstructure. The microstructural characteristics in terms of residual stress, XRD patterns, phase composition and content, and nano-scale crystallite size of machined surface layer were characterized to reveal the machined surface layer quality adjustment and controlling mechanism from the prospective of the microscopic scale. The experimental results showed that the cutting force and compressive residual stress were larger at low roughing cutting speed than that at high roughing cutting speed because of the combined effects of mechanical and thermal deformations. In the two-step machining process, with the increase of roughing cutting speed, the β phase on the finishing surface firstly increased and then decreased. Meanwhile, the high roughing cutting speed weakened the microcrystal refinement of the finishing surface because of the work hardening effect. Therefore, the appropriate roughing machining parameters will contribute to the improvement of finishing machined surface quality in the terms of lower cutting force, higher compressive residual stress, and better grain refinement, phase content, and preferred crystallite orientation, thus increasing the microscopic mechanical properties of machined surface layer. This provides a reference for optimizing the cutting parameters to adjust and control the quality and integrity of the machined surface layer in two-step milling of Ti-6Al-4V alloy.

Keywords Two-step milling · Titanium alloy · Machined surface quality · Microscopic mechanism

1 Introduction

Titanium alloys are widely used in aerospace, military industry, medical equipment, and other fields for their excellent properties such as high specific strength, corrosion resistance, and good thermal stability [1–3]. However, titanium alloy Ti-6Al-4V is a typical difficult-to-machine material, which is difficult to machine due to its low thermal conductivity and low elastic modulus, and the quality of machined surface is difficult to guarantee [4, 5].The service life and performance of components are highly related to the quality of machined surface, so the control of machined surface quality has always been an important research direction in the field of metal cutting [6]. In the cutting process, the workpiece is affected by cutting heat, cutting force, and friction, which leads to the microstructure change of the machined surface layer, such as the grain elongation, slip, and fragmentation, and the residual stress of the surface layer is also affected. By studying the influence mechanism of surface roughness, work hardening, residual stress, microstructure, and other important components of machined surface quality, we can optimize machining parameters, improve machining technology, and obtain ideal machined surface quality [7–9]. The surface quality is affected by many factors, especially cutting parameters, cutting tool parameters, tool wear, machining methods, and so on [10–12], among

✉ Anhai Li
anhaili@sdu.edu.cn

1 Key Laboratory of High Efficiency and Clean Mechanical Manufacture of MOE, School of Mechanical Engineering, Shandong University, Jinan 250061, People's Republic of China

2 National Demonstration Center for Experimental Mechanical Engineering Education (Shandong University), Jinan 250061, People's Republic of China

which the effect of cutting parameters on surface quality is a complex and multi-factor process. At present, the research on surface quality mainly focuses on the single-step machining process.

However, in the actual machining process, most integral structural components cannot be machined by one-step machining. The surface quality of finishing is inevitably affected by roughing parameters. The service performance of finished components depends not only on the finishing steps, but also on the whole cutting process. Obviously, it is of great significance to study not only the cutting parameters of finish machining, but also the influence of rough machining parameters and cutting steps on finish machining in the whole machining process. However, the selection of rough machining parameters in the process of surface quality adjustment and control of titanium alloy machining is still based on experience and analogy, lacking systematic scientific experimental basis [13]. At the same time, the service environment also requires the adjustment and control of residual stress distribution on the machining surface of titanium alloy integral structural components. Hou et al. [14] studied the effect of rough cutting parameters on cutting force, surface roughness, residual stress, and surface topography in the finishing process by multi-step turning of titanium alloy Ti-6Al-4V and analyzed the effect of the previous step on the next step in multi-step cutting process. The results showed that the cutting speed of rough machining had the greatest influence on the cutting force and surface roughness of finish machining.

Residual stress is an important part of machined surface integrity, which has an important influence on the service life and fatigue resistance. The results of cutting titanium alloys Ti-6Al-4V and Ti-6Al-2Sn-4Zr-6Mo [15] showed that cutting speed, feed rate, and arc radius had obvious effects on surface residual stress. Sun and Guo [16] pointed out that the increase of feed rate led to the increase of surface residual tensile stress in the high-speed milling experiment. Sridhar et al. [17] studied the influence of different cutting parameters and cutting temperature on residual stress. The results indicated that the residual stress decreased with the increase of cutting depth and increased with the increase of cutting speed.

Different cutting sequences in multi-step machining process can change the residual stress distribution on the machined surface. Strain accumulation and temperature in cutting process led to great changes in residual stress distribution of machined surface layer [18]. Reasonable number of cutting steps and parameters setting are beneficial to obtain residual stress which can improve the service performance of manufactured components. Zlatin and Field [19] found that roughing produced tensile residual stress on the workpiece surface, while finish machining was beneficial to the generation of compressive residual stress. Sasahara et al. [20] studied the influence of the previous step on the residual stress of the following step in the multi-step cutting process. The experimental and simulation results showed that the surface residual stress can be improved by adjusting the proper cutting sequence.

The change of macroscopic properties of titanium alloy depends on the change of microstructure. The investigation on the change of microstructure of machined surface of titanium alloy could effectively control and improve the quality of machined surface [21]. In the traditional research of metal cutting mechanism, the experimental phenomena were generally explained by macroscopic force, thermal phenomena, and geometric principles. With the development of observation means and equipment, micromechanism had been introduced into metal cutting research. A series of studies on microscopic mechanisms, such as crystallographic orientation texture, phase transformation, and grain refinement, were used to understand the cutting process more deeply and guide the more scientific optimization of machining parameters [22]. At the same time, microscopic mechanism research was also combined with the vigorous development of finite element simulation to achieve a more accurate prediction model. The visco-plastic self-consistent (VPSC) program developed by Huang [23] based on crystal plastic constitutive promoted the application of crystal plastic theory in cutting. Based on the theory of crystal plasticity, Wang and Liu [24] studied the influence of strain change on the evolution of crystallographic texture during high-speed cutting of titanium alloy. The results showed that with the increase of cutting speed, the equivalent strain and cutting temperature increased, which led to the formation of C-type texture. Li et al. [25] established a polycrystalline plastic finite element model to study the plastic deformation and texture evolution of the machined surface of Ti-6Al-4V titanium alloy. Typical columnar texture and shear texture were found on the machined surface, and the texture orientation density decreased with the increase of cutting speed.

Severe plastic deformation and high temperature occur in the cutting process, and then, the workpiece is rapidly cooled to room temperature, which is accompanied by the mutual transformation of α phase and β phase. Wang et al. [26] established stress-temperature phase transformation model based on phase transformation dynamics to study the relationship between cutting parameters and phase transformation in Ti-6A1-4V high-speed machining. The simulation results showed that α phase to β phase transformation occurred at higher cutting speeds. Plastic deformation in cutting process led to grain elongation and breakage, and promoted grain refinement, but the cutting heat could promote grain growth and inhibit grain refinement. Pan et al. [27] simulated the cutting residual stress of titanium alloy Ti-6Al-4V with a microstructural consideration, and analyzed the grain size distribution of α phase under different cutting speeds and feed rates by electron back scattered diffraction (EBSD). It was found that there was obvious grain growth on the machined surface layer of the workpiece.

Titanium alloy integral structural components have high material removal rate and high machining difficulty, which require multi-step cutting. Meanwhile, the requirements for residual stress distribution on the finished surface are also strict, and scientific methods for surface quality adjustment and control of the machined surface are needed. Most of the existing researches on multi-step cutting are about macroscopic surface quality, so it is of great significance to study the distribution of residual stress and phase under the machined surface of previous cutting step and the change of grain size caused by the change of two-step milling parameters. In this paper, the influence of different roughing parameters on the cutting force of roughing and finishing as well as the residual stress of finishing surface was studied by two-step milling of titanium alloy. At the same time, the effect of rough machining parameters on the microstructure of roughing and finishing surface layer was studied, especially from the following aspects of the phase composition, phase distribution, and nano-scale crystallite size. The diffraction patterns of machined surface layer under different machining conditions obtained by X-ray diffraction (XRD) technique and the phase distribution were analyzed. The Schemer equation was used to calculate the nano-scale crystallite size. The effect of the variation of cutting parameters of roughing and finishing on the surface microstructure was revealed. The research on microscopic mechanism of surface quality adjustment and control of titanium alloy machining is of great significance to improve the surface quality.

2 Two-step milling experiment of titanium alloy

2.1 Workpiece materials and experimental conditions

The workpiece material used in the experiment was $\alpha+\beta$ two phase titanium alloy Ti-6Al-4V. The composition of this material is shown in Table 1. The machining samples were Ti-6Al-4V titanium alloy blocks with dimensions of 100 mm × 75 mm × 30 mm. Titanium alloy was machined in two-step by down milling.

The experimental setups of the cutting tests are shown in Fig. 1. A series of milling experiments were conducted on a DAEWOO ACE V500 three-axis vertical machining center with, with FANUC 18 numerical control system and a maximum spindle rotation speed of 10,000 rpm. The detailed equipment of milling operation is shown in Fig. 1a, and the schematic diagram of two-step rough/finish machining process is shown in Fig. 1b. The type of milling cutter tool holder (Fig. 1d) is R217.69–2525.0–09-3AN produced by SECO cutting tool company, and the tool inserts are CVD Ti(C, N)-Al_2O_3 coated ultra-fine carbide with type XOMX090308TR-M08, MP2500. The geometric shape and parameters of cutting tools are shown in Fig. 1e. Rough machining and finish machining had the same tool settings.

The roughing parameters of two-step milling experiment are listed in Table 2. In order to reduce the influence of tool wear, new tools were used for each cutting experimental trials. Four passes per cutting step to ensure the reliability of experimental data. During the milling experiment, the axial cutting depth a_{p1} and a_{p2} of roughing and finishing were both 1 mm. During the whole milling experiment, the finishing cutting parameters were constant, and the cutting process was conducted at the cutting speed of $v_2 = 280$ m/min, radial cutting depth of $a_{e2} = 0.2$ mm, and feed rate of $f_{z2} = 0.05$ mm/z under dry cutting conditions. In order to reflect the influence of roughing on finishing, the radial cutting depth a_{e2} of finishing was set to be significantly smaller than roughing. The first to seventh groups of experiments in Table 2 showed that the roughing cutting speed increases in turn. In the 8th, 6th, 9th and 10th groups of experiments, the radial cutting depth a_{e1} of roughing increased in turn. In the 11th, 6th and 12th groups of experiments, the feed rate f_{z1} per tooth in roughing increased in turn.

2.2 Measurement of cutting force

Cutting force is a basic physical quantity reflecting the essential state of cutting process, which can characterize the advantages and disadvantages of cutting process, and is closely related to mechanical deformation and thermal deformation in cutting process. In the two-step side milling cutting process, a Kistler 9257B dynamometer equipped with 5697A signal collector, 5070A signal amplifier, and DynoWare signal processing software (exhibited in Fig. 1c) was used to measure the cutting force. The dynamometer recorded the three coordinate forces, which were the main milling force F_c, the vertical milling force F_{cN}, and the back force F_p. After removing the unstable experiment data in the cutting process, the average peak values of 20 main milling force curves were taken as the steady main cutting force, and the standard deviation was calculated as error bar.

Table 1 Chemical composition of titanium alloy Ti-6Al-4V

Elements	Al	V	Fe	C	N	H	O	Other	Ti
Weight (wt%)	5.5–6.75	3.6–4.5	0.3	0.08	0.05	0.15	0.1	0.5	Base

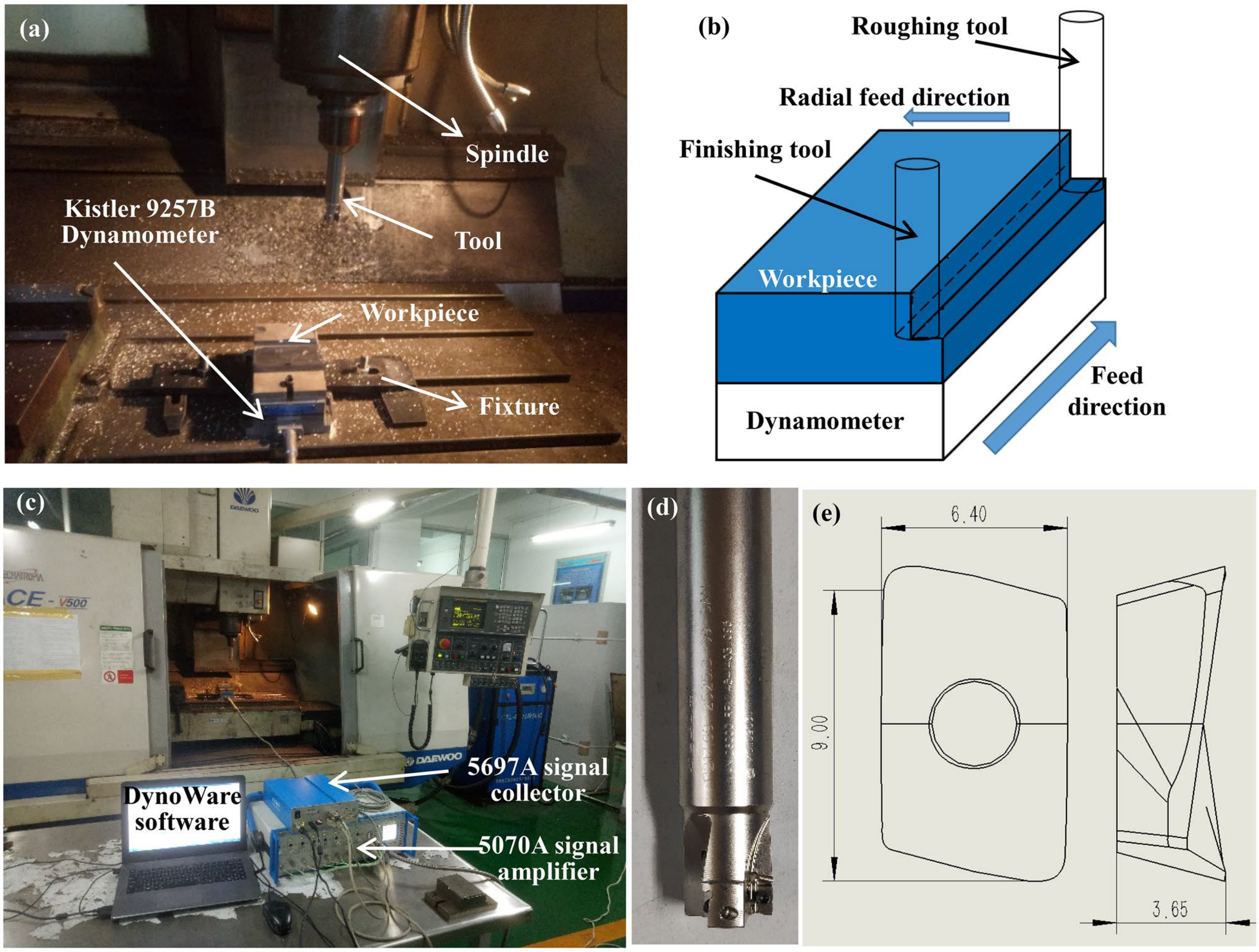

Fig. 1 Experimental setups. (**a**) Experiment equipment, (**b**) schematic diagram of two-step milling process, (**c**) setting of milling force detection device, (**d**) cutting tool holder, (**e**) cutting tool insert geometry

Table 2 Roughing cutting parameters of two-step machining

Level	Cutting speed v_1 (m/min)	Radial cutting depth a_{e1} (mm)	Axial cutting depth a_{p1} (mm)	Feed rate f_{z1} (mm/z)
1	80	1	1	0.05
2	120	1	1	0.05
3	160	1	1	0.05
4	200	1	1	0.05
5	240	1	1	0.05
6	280	1	1	0.05
7	320	1	1	0.05
8	280	0.5	1	0.05
9	280	1.5	1	0.05
10	280	2	1	0.05
11	280	1	1	0.03
12	280	1	1	0.07

2.3 Measurement of residual stress

The volume change caused by non-uniform deformation, thermal deformation, and phase transformation influences the residual stress. For cutting process, it is generally considered that cutting residual stress is related to plastic strain caused by mechanical stress and thermal stress. The research showed that when the machined surface appeared compressive residual stress, it was beneficial to improve the corrosion resistance and fatigue strength of the material [28].

X-ray diffraction, as a non-destructive residual stress detection method, was used to examine the residual stress on the machined surface [29]. Residual stress was measured by XSTRESS3000X X-ray stress analytical instrument. After the two-step milling experiment of titanium alloy was completed, the samples were cut off by wire electrical discharge machine for subsequent measurement. Based on X-ray diffraction crystallography theory and elasticity theory, the residual stress of the machined surface of the sample was

Table 3 Parameters of residual stress detection on machined surface

Items	Values
Workpiece material	Ti-6Al-4V alloy
Measuring voltage (kV)	30
Measuring current (mA)	6.7
Gain voltage (kV)	16
Exposure time (s)	10
Exposure times	4
Diffraction lattice plane *hkl*	*110*
Angle between *X* ray incident ray and normal line of pattern surface ψ	0° ± 5.55° ± 11.48° ± 19.29° ± 24.8° ± 30°
Collimator diameter (mm)	2
Elastic modulus (GPa)	120.2
Poisson's ratio	0.36
Stress constant (MPa/°)	1750.39
Diffraction angle of unstressed Ti powder 2θ (°)	139

measured, and the samples were measured three times and averaged to reduce the error. Ti-Kα target was used in the detection experiment. The detailed detection parameters are set as shown in Table 3. Before formal measurement, stress-free Ti powder calibration was used to determine the appropriate measuring distance between the collimator and the machined surface.

2.4 XRD detection

X-ray has a short wavelength, which can interact with periodic crystalline matter and enhance coherence in some directions. Therefore, strong X-ray diffraction can be generated in some specific directions, and the orientation and intensity of its spatial distribution can reflect the crystallite structure [30].The machined surface was cut off by wire electrical discharge machine, and the two-step machined surface was measured by XRD using D8 Advance X-ray diffractometer produced by Brook Company in Germany.

XRD analysis is based on Bragg equation shown in Eq. (1). The intensity, width, and location of XRD diffraction peak change with the microstructure of the material, such as dislocation density, lattice distortion, and crystallite size. Therefore, by analyzing the XRD diffraction pattern, the nano-scale crystallite size can be calculated by Bragg equation [31, 32]:

$$2d\ \sin\theta = n\lambda \tag{1}$$

where d is the interplanar spacing (m), θ is the half of Bragg diffraction angle (°), n is reflection series, and λ is the wavelength of the X-ray beam (0.6 ~ 20 angstroms).

The Scherrer equation related the crystallite diameter along the direction perpendicular to the crystal plane with diffraction data. The crystallite block size D_{hkl} (nm) perpendicular to the diffraction direction of the crystal lattice plane (*hkl*) can be expressed as Scherrer equation:

$$D_{hkl} = k\lambda/\omega cos\theta \tag{2}$$

where k is the Scherrer constant (usually 0.89), λ is the incident X-ray wavelength (generally the wavelength of Cu $K\alpha$ is 0.154056 nm), and ω is the full width at half maximum (FWHM, rad) of diffraction peak.

The calculation process of crystallite size using XRD data can be roughly divided into four steps: diffraction peak correction, FWHM extraction, unit conversion, and Scherrer equation calculation. The method of calculating crystallite size by Eq. (2) was very sensitive to the diffraction peak intensity, so α-Ti (101) plane with higher intensity was selected for calculation. Figure 2 is a schematic diagram of FWHM of the bulk material and diffraction angle 2θ. The FWHM (rad) and diffraction angle 2θ (°) of α-Ti (101) plane extracted from roughing and finishing surface layer were located and measured by Jade software.

3 Results and discussions

3.1 Cutting forces

The main milling forces under different cutting parameters in rough machining are shown in Fig. 3. It could be seen from Fig. 3a that with the increase of cutting speed, the cutting force first increased and then decreased, with the maximum cutting force appearing at 120 m/min and the minimum

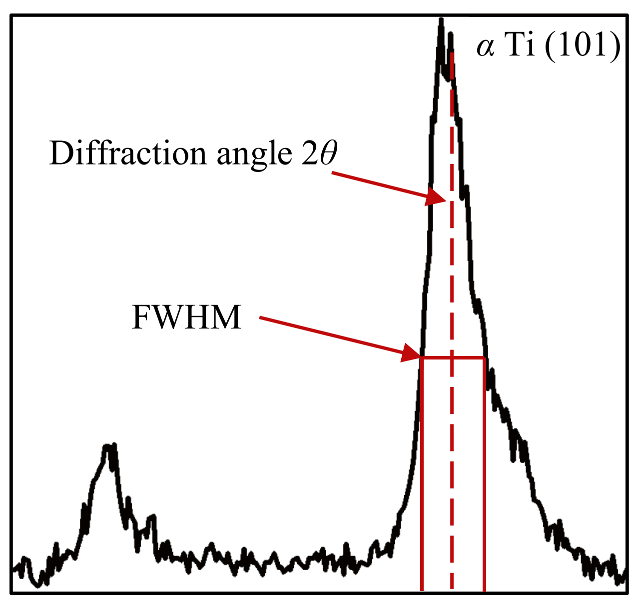

Fig. 2 Diagram of FWHM and diffraction angle 2θ of titanium alloy

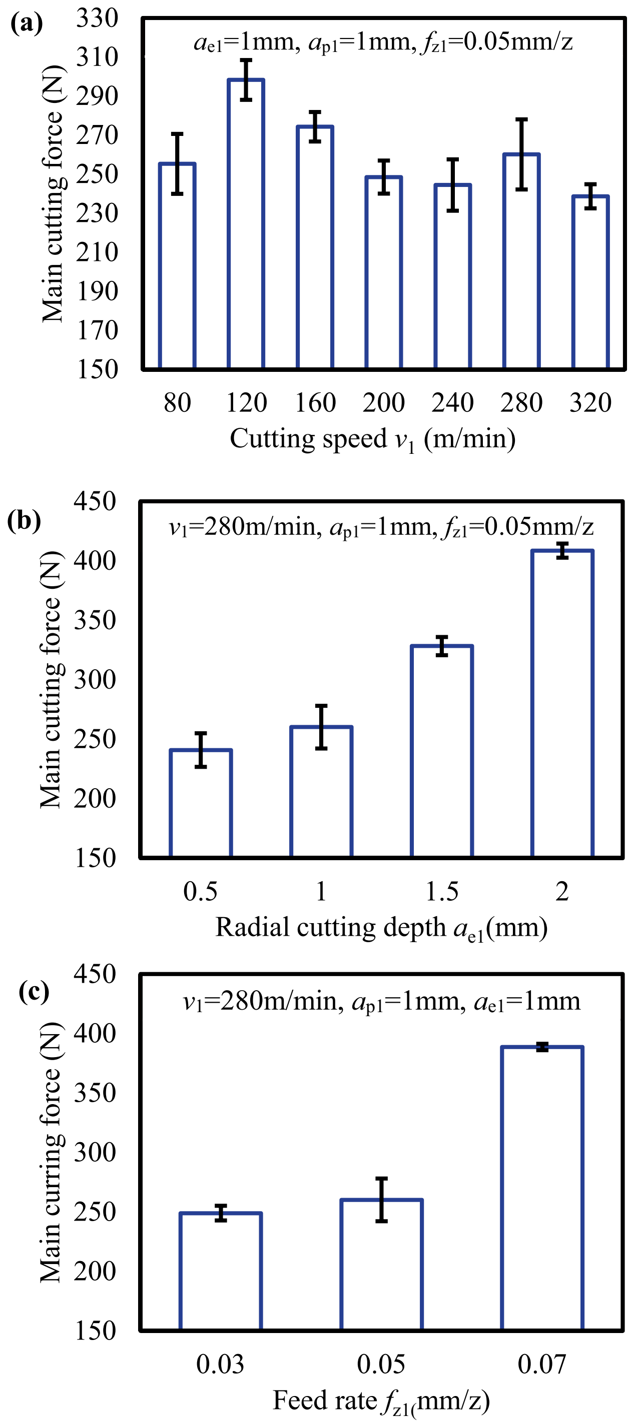

Fig. 3 Effect of cutting parameters on main cutting force in rough machining (**a**) cutting speed v_1, (**b**) radial cutting depth a_{e1}, and (**c**) feed rate f_{z1}

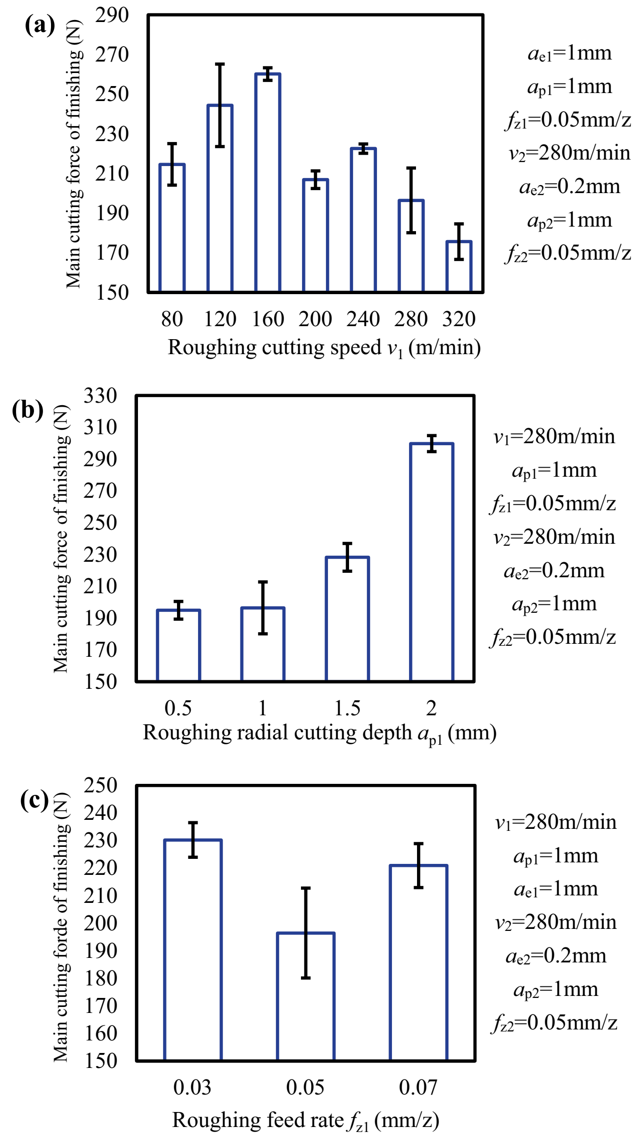

Fig. 4 Effect of roughing cutting parameters on main cutting force of finishing (**a**) cutting speed v_1, (**b**) radial cutting depth a_{e1}, and (**c**) feed rate f_{z1}

cutting speed at 320 m/min. It can be seen from Fig. 3b that with the increase of radial cutting depth a_{e1}, the cutting force showed a monotonically increasing trend, and the radial cutting depth a_{e1} reached the maximum value at 2 mm. As shown in Fig. 3c, other cutting parameters of roughing are fixed, and the variation of roughing cutting force is studied by changing the feed rate. With the increase of feed rate in roughing, the cutting force in roughing first stabilized at a value and then increased. The maximum cutting force of roughing appeared when the feed rate was 0.07 mm/z.

Figure 4 shows the effect of roughing parameters on the main cutting force of finishing. In Fig. 4a, it can be observed that when the rough machining speed was less than 160 m/min, the cutting force of finish machining showed an obvious upward trend, and the roughing speed continued to increasing. While the rough machining cutting speed continued to increase, and the finishing cutting force generally showed a downward trend except for the fluctuation at roughing

240 m/min, the maximum value of cutting force appeared at the cutting speed of 160 m/min and the minimum value appeared at the cutting speed of 320 m/min, which was 46% lower than the maximum value at 160 m/min.

The cutting force mainly comes from that resistance produce by the elastic–plastic deformation of materials during the cutting process and the friction force between the tool and the chip and the workpiece surface. Under the same cutting parameters, the greater the hardness, shear yield strength and toughness of the material were, the greater the cutting force was. In the roughing process, due to the effect of plastic deformation and cutting heat, the strength and hardness of the machined surface layer of the workpiece were improved, and then, the hardening occurred [33].The work hardening layer changed the material characteristics of the surface to be machined, which led to the increase of cutting force in finishing. However, the variation of roughing parameters caused different hardening degree, which made different changes in finishing cutting force. Previous studies had shown that with the increase of cutting speed, the hardness of machined surface and surface at a certain depth first increased and then decreased [18]. It can be inferred that when the cutting speed increased from 80 to 160 m/min, the work hardening effect increased, which led to the increase of the surface hardness of the workpiece at the beginning of finishing and then led to the increase of cutting force and the deterioration of the machined surface quality such as roughness.

When the cutting speed was greater than 160 m/min, the cutting heat was greatly increased, and the thermal softening effect was significantly enhanced, which weakened the hardening effect, reduced the hardness of the machined surface, and then led to the reduction of cutting force. However, because of the poor thermal conductivity of titanium alloy, the plastic deformation at 240 m/min is greater than the thermal softening effect, resulting in the fluctuation of finishing cutting force. In the cutting process, in the high cutting speed stage (above 160 m/min), the roughing cutting speed can be increased as much as possible, and the lower finishing cutting force can be obtained. However, because of the poor thermal conductivity, the plastic deformation at 240 m/min had a greater impact than the thermal softening effect, resulting in the fluctuation of finishing cutting force. In order to get lower finishing cutting force, the roughing cutting speed can be increased as much as possible during high-speed cutting (above 160 m/min).

It can be seen from Fig. 4b that the cutting force in finishing increased as the radial cutting depth in roughing increased. When the radial cutting depth of rough machining reached 2 mm, the cutting force of finishing increased obviously and reached the maximum value compared with roughing at the radial cutting depth ae1 of 0.5 mm, 1 mm, and 1.5 mm. Previous studies had shown that the increasing of cutting depth led to the intensification of work hardening effect on the workpiece surface, and at a certain depth, the hardness was improved [34]. It was concluded that the work hardening was not obvious when the radial cutting depths of roughing were 0.5 mm, 1 mm, and 1.5 mm, but obvious work hardening occurred when the radial cutting depth reached 2 mm, which resulted in a significant increase in cutting force of finishing. Figure 4c shows that with the increase of roughing cutting speed, the cutting force of finishing first decreased and then increased, but the change range was not large. This is because the change of roughing cutting feed had limited effect on rough machining surface hardening, and then had no obvious effect on the variation of cutting force of finishing.

3.2 Residual stress of the machined surface

Rough machining plastic strain causes hardening of the surface to be machined, and the cutting heat causes thermal softening of the finishing surface to be machined. On the other hand, the residual stress of the finishing surface was affected by the residual stress produced by the rough machining surface. Figure 5 shows the effects of the roughing cutting parameters on residual stress on the finishing surface under the condition of fixed finishing cutting parameters. Each sample was tested for 3 times and averaged to reduce the error. The experiment results showed that the residual stress on all finishing surfaces was compressive residual stress.

The effect of roughing cutting speed v_1 on the residual stress on the finishing surface is shown in Fig. 5a. Compared with other cutting speeds, the compressive residual stress on the finishing surface was larger at lower roughing cutting speeds (80 m/min, 120 m/min), and the maximum compressive residual stress was −333.94 MPa at the cutting speed of 120 m/min. Under the condition of high roughing cutting speed (160 m/min ~ 320 m/min), the compressive residual stress was obviously smaller than that at low roughing cutting speed, and it increased at first and then decreased. When roughing cutting speed was 240 m/min, it was the maximum compressive residual stress in high-speed cutting section, and its value was −169.03 MPa.

After rough machining, the machined surface was affected by plastic deformation and cutting heat, resulting in work hardening and thermal softening. With the increase of roughing cutting speed, the work hardening effect weakened. On this basis, the surface to be machined was weakened by the work hardening effect, and then, the compressive residual stress decreased. At the same time, the cutting force of finishing was large under the condition of low roughing cutting speed, and the compressive residual stress of finishing surface increased due to the extrusion effect. With the increase of roughing cutting speed, the cutting force of finish machining decreased, and the compressive residual

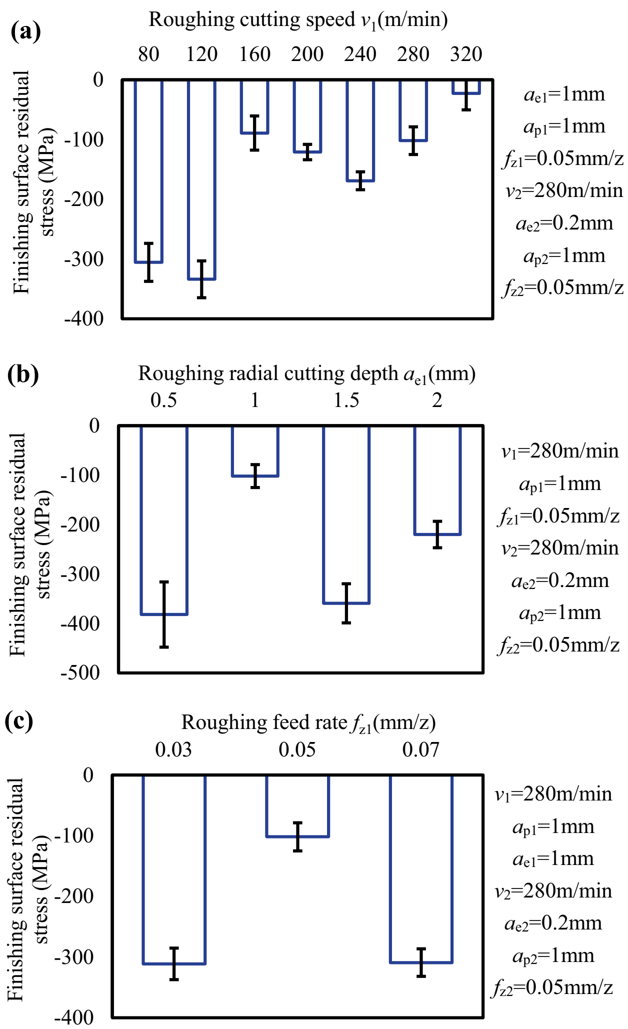

Fig. 5 Effect of roughing cutting parameters on residual stress of finishing (**a**) cutting speed v_1, (**b**) radial cutting depth a_{e1}, and (**c**) feed rate f_{z1}

stress of finishing surface decreased due to the weakening of the extrusion effect. Therefore, a lower cutting speed was recommended to use for rough machining in order to obtain larger compressive residual stress in the two-step milling process. The cutting speed should be as close as possible to 240 m/min in high-speed cutting process, and higher cutting speed will lead to an obvious reduction of compressive residual stress.

Figure 5b shows the residual stress of finishing surface with variable roughing radial cutting depth a_{e1}. Under the cutting speed of 280 m/min, among the four radial cutting depth parameters of 0.5 mm, 1 mm, 1.5 mm, and 2 mm, the minimum compressive residual stress at 1 mm radial cutting depth was −101.91 MPa. The maximum residual compressive stress was −381.90 MPa at the cutting depth of 0.5 mm. Because rough machining has the weakest work hardening effect on the surface to be machined, the material is easy to

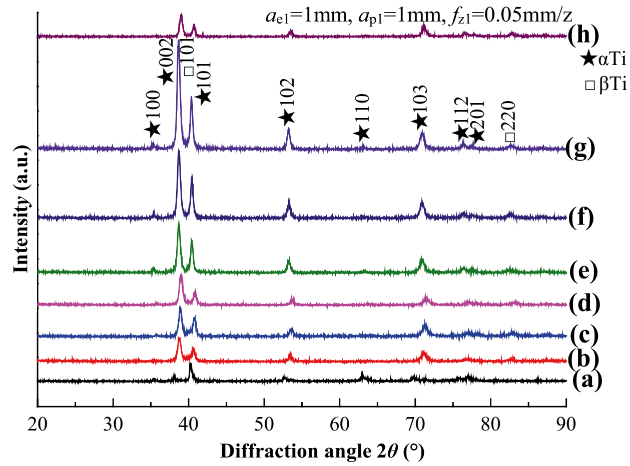

Fig. 6 Effect of cutting speed on XRD pattern of Ti-6Al-4V alloy (**a**) bulk material, (**b**) $v_1 = 80$ m/min, (**c**) $v_1 = 120$ m/min, (**d**) $v_1 = 160$ m/min, (**e**) $v_1 = 200$ m/min, (**f**) $v_1 = 240$ m/min, (**g**) $v_1 = 280$ m/min, (**h**) $v_1 = 320$ m/min

present residual compressive stress. Through the analysis, in the two-step cutting process, in order to obtain larger compressive residual stress on the finishing surface, it is necessary to adopt a lower radial cutting depth (0.5 mm), and when the radial cutting depth was larger, it was necessary to reach the radial cutting depth of 1.5 mm as far as possible.

Figure 5c shows the variation of the residual stress of finishing surface by changing the feed rate f_{z1} in rough machining. With the increase of feed rate f_{z1} in roughing, the compressive residual stress in finishing firstly decreased and then increased. The maximum compressive residual stress appeared at the feed rate f_{z1} of 0.03 mm/z in rough machining and reached to the value −311.44 MPa. The compressive residual stress was the smallest when the feed rate f_{z1} was 0.05 mm/z.

3.3 XRD pattern and phase composition of machined surface layer

X-ray diffraction pattern detection results are shown in Figs. 6, 7, 8, 9, 10, and 11. The diffraction data of peak position, shape, and intensity changes caused by α-Ti and β-Ti phases were analyzed. The diffraction angle 2θ of each XRD pattern ranged from 20° to 90°, which clearly showed planes (100), (002), (101), (102), (110), (103), (112), and (201) of α-Ti and plane (101) of β-Ti in turn.

As shown in Fig. 6, compared with the bulk material, the diffraction peak position of the machined surface obviously shifts to a larger or smaller angle. It was indicated that residual stress appeared on the machined surface, which led to microdistortion and position shift. At first, the diffraction intensity of the overlapping peaks of α-Ti (002) plane and β-Ti (101) plane was less than that of α-Ti (101) plane. After

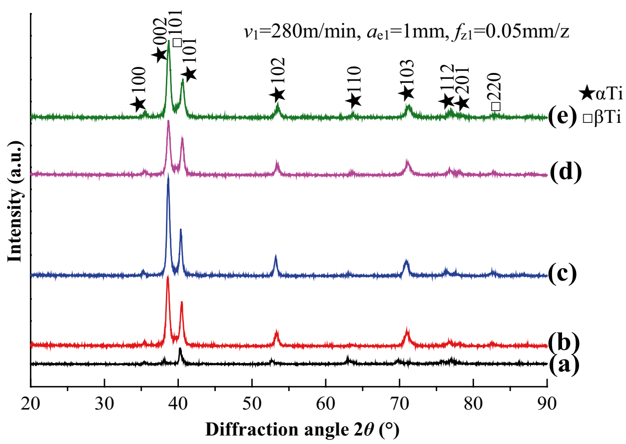

Fig. 7 Effect of radial cutting depth on XRD pattern of Ti-6Al-4V alloy (**a**) bulk material, (**b**) $a_{e1} = 0.5$ mm, (**c**) $a_{e1} = 1$ mm, (**d**) $a_{e1} = 1.5$ mm, (**e**) $a_{e1} = 2$ mm

machining, the diffraction intensity of overlapping peaks of α-Ti (002) plane and β-Ti (101) plane on each machined surface is significantly higher than that of α-Ti (101) plane. By comparing the peak intensity of the two diffraction peaks, it was found that a new β phase was formed and the surface β phase increased during cutting process. Obvious work hardening appeared on the machined surface in the cutting process, which led to surface grain refinement, crystallite refinement, and high-density dislocation. The crystallite size is closely related to the variation of diffraction peak width. Therefore, the diffraction peak width was closely related to the material structure, work hardening, and microstress. The variation of microstructure caused the change of microhardness and diffraction peak width. The more severe the plastic deformation of the machined surface was, the more obvious the crystallite refinement was.

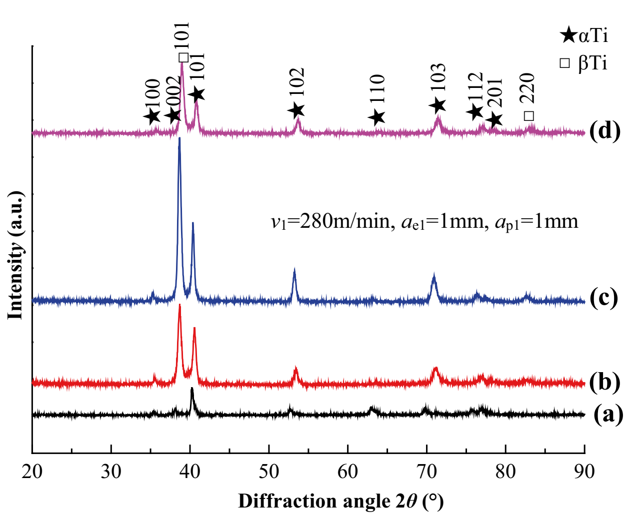

Fig. 8 Effect of feed rate on XRD pattern of Ti-6Al-4V alloy (**a**) bulk material, (**b**) $f_{z1} = 0.03$ mm/z, (**c**) $f_{z1} = 0.05$ mm/z, (**d**) $f_{z1} = 0.07$ mm/z

Furthermore, the diffraction peak width of the machined surface was obviously larger than that of the bulk material (Fig. 6a). Severe plastic deformation on the machined surface during the machining process caused grain refinement and surface dislocation and lattice distortion. Meanwhile, internal stress was generated between grains and crystallites, and the diffraction peak width of the machined surface was widened [35]. At the same time, with the increase of cutting speed, the diffraction peak width decreased slightly. This phenomenon indicated that the plastic deformation tended to decrease. When the roughing cutting speed was within the range of 80 to 280 m/min, the diffraction peak intensity was stronger than the bulk material peak intensity, and it was constantly increasing, which indicated that the crystallinity of the machined surface was increasing. When machining at the cutting speed of 320 m/min, the intensity of diffraction peak decreased obviously, and the increase trend of crystallinity was interrupted.

Figure 7 shows the influence of radial cutting depth on X-ray diffraction pattern of machined surface. It can be seen from Fig. 7 that the intensity and width of diffraction peaks changed slightly under different radial cutting depths, but they were obviously larger than those of the bulk material. The deviation of diffraction peaks also indicated the existence of residual stress.

It can be seen from Fig. 9 that the diffraction peak deviation degree of the finishing surface was more obvious when the roughing cutting speed was 80 m/min and 120 m/min than that under other cutting conditions, which confirmed the conclusion that the compressive residual stress value of the finishing surface was larger under the condition of low roughing cutting speed. However, under the condition of higher cutting speed, the partial deviation returned to the diffraction peak position of the bulk material, which showed that the residual stress in finishing at this time was not as obvious as that under the condition of low roughing cutting speed.

Figure 11 shows the influence of roughing feed rate on XRD pattern of finishing surface. When roughing feed rate was 0.03 m/z, the diffraction intensity of α-Ti (101) plane was stronger than that of the overlapping peak of α-Ti (002) plane and β-Ti (101) plane. After that, the overlapping peaks of α-Ti (002) plane and β-Ti (101) plane reversed the diffraction peaks of α-Ti (101) plane, which reflected the obvious increase of β phase with the rough machining parameters varying from 0.03 to 0.05 mm/z. When the feed rate in rough machining was 0.03 mm/z, the diffraction peak position offsets more seriously than that of the bulk material, which verified the rule that the compressive residual stress on the finishing surface was the largest in the residual stress detection. Compared with other diffraction peaks, the peak intensity

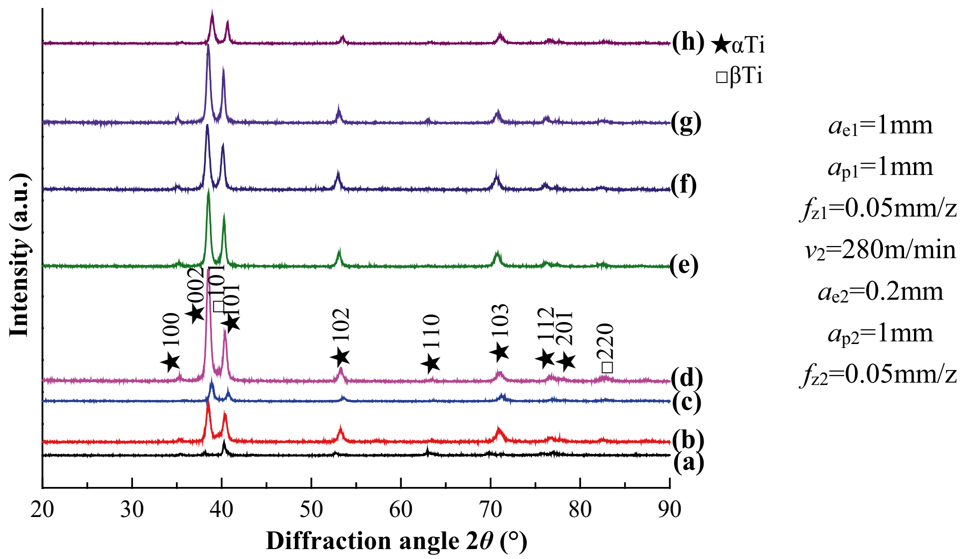

Fig. 9 Effect of roughing cutting speed on XRD pattern of finishing surface (**a**) bulk material, (**b**) $v_1 = 80$ m/min, (**c**) $v_1 = 120$ m/min, (**d**) $v_1 = 160$ m/min, (**e**) $v_1 = 200$ m/min, (**f**) $v_1 = 240$ m/min, (**g**) $v_1 = 280$ m/min, (**h**) $v_1 = 320$ m/min

of α-Ti (002) plane on the machined surface increased most obviously, which indicated that C-plane (00 l) texture appeared on the machined surface. On the other hand, the (*hk0*) crystal plane such as α-Ti (100) plane and (110) plane had no obvious increase compared with other diffraction peaks, which indicated that the texture of the (hk0) crystal plane was not obvious in the actual cutting process.

3.4 Phase content of machined surface layer

Rough machining caused severe plastic deformation on the surface to be machined, and changed the stress distribution of the machined surface, which led to hardening of the machined surface. The machined surface was also affected by the cutting heat in the rough machining process. In order to reveal the influence of rough machining on the surface phase distribution of finishing, it is necessary to make a further quantitative analysis of the phase content changes reflected by diffraction patterns. The law of phase distribution in cutting process can be obtained from XRD pattern. The phase content was calculated according to the intensity of each diffraction peak.

Ti-6Al-4V is a typical α-β dual phase titanium alloy. However, the untreated Ti-6Al-4V titanium alloy has an absolute majority of α phase with HCP structure at room temperature, and the β phase content is less than 10% [36].

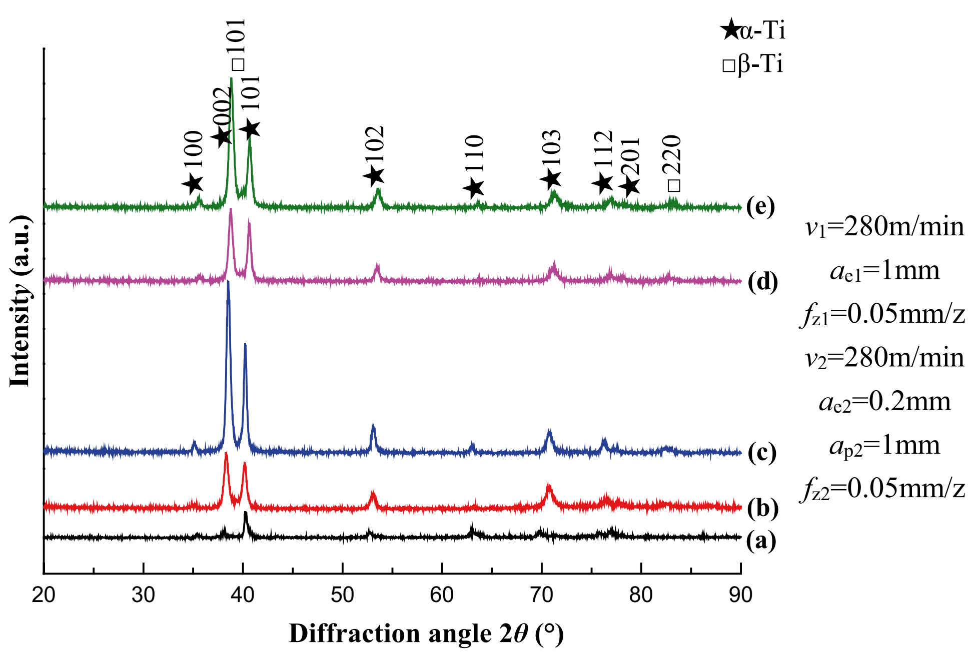

Fig. 10 Effect of roughing radial cutting depth on XRD pattern of finishing surface (**a**) bulk material, (**b**) $a_{e1} = 0.5$ mm, (**c**) $a_{e1} = 1$ mm, (**d**) $a_{e1} = 1.5$ mm, (**e**) $a_{e1} = 2$ mm

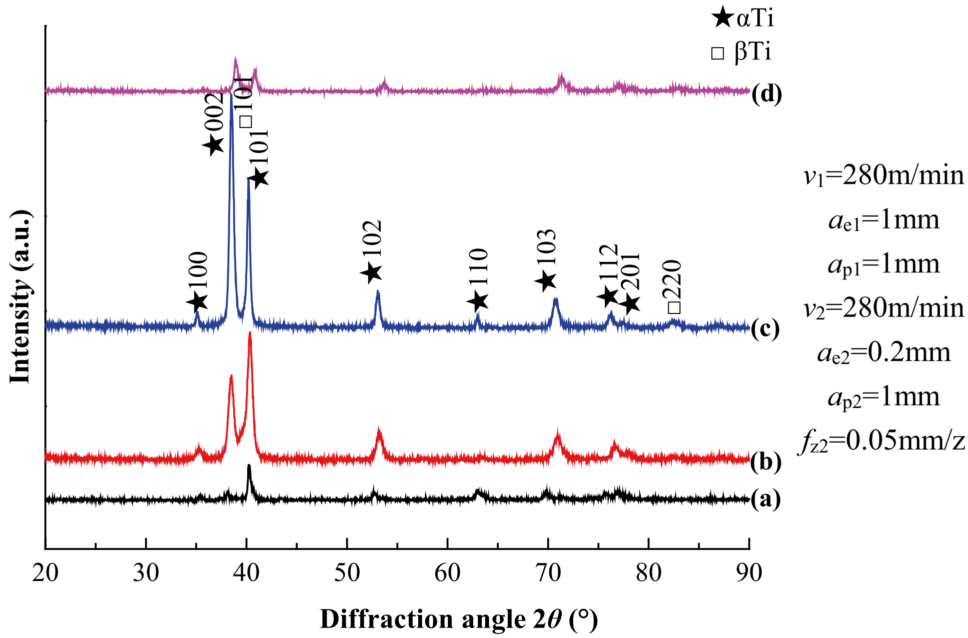

Fig. 11 Effect of roughing feed rate on XRD pattern of finishing surface (**a**) bulk material, (**b**) $f_{z1}=0.03$ mm/z, (**c**) $f_{z1}=0.05$ mm/z, (**d**) $f_{z1}=0.07$ mm/

When the temperature reaches 882.5 ℃ which is the initial point of transformation temperature, α phase begins to transform into β phase with BCC structure. During the cooling process, with different cooling rates, different degrees of β phase to α phase transformation occur [37]. In the cutting process, high temperature and high pressure are generated between the tool and the workpiece, and the temperature in the second deformation zone reaches the initial point of transformation temperature, which leads to the transformation of α-Ti into β-Ti on the machined surface. After the tool leaves the workpiece surface, the workpiece cools rapidly, and the transformation from β-Ti to α-Ti takes place in different degrees [38, 39]. The change trend of phase distribution can be analyzed by studying the results of phase distribution under different cutting conditions.

Figure 12 shows the effect of variable cutting parameters on the distribution of α-Ti and β-Ti on the machined surface. It can be seen from Fig. 12 that the bulk material phase content of Ti-6Al-4V titanium alloy was 92.3% α phase and 7.7% β phase. The research showed that during the cutting process, the transformation from α phase to β phase occurred in the rapid heating process and the transformation from β phase to α phase occurred in the rapid cooling process [40]. It can be seen from Fig. 12a that with the increase of cutting speed v_1, the contents of α phase and β phase on the machined surface had little change compared with the bulk material, and the maximum value of β phase appeared at the cutting speed of 160 m/min (15.5%). It is proved that the transformation from α phase to β phase in heating process is greater than that from β phase to α phase in rapid cooling process. The minimum β phase content was 10.9% at the cutting speed of 200 m/min. With the cutting speeds increase to the range between 200 and 320 m/min, the β phase content increased slightly, and the increasing trend remained unchanged. The β phase content reached 13.6% at the cutting speed of 320 m/min.

It can be seen from Fig. 12b that different radial cutting depths ae1 had little effect on the phase distribution of the machined surface, and the β phase content fluctuated slightly. It can be seen from Fig. 12c that with the increase of feed rate f_{z1}, compared with the bulk material phase content, the β phase content had little change, but the β phase content increases obviously with the increase of feed rate f_{z1}. The β phase content on the machined surface affected by cutting process was greater than that of the bulk material.

Figure 13 shows the influence of roughing parameters on the phase distribution of the finishing surface. It can be seen from Fig. 13a that with the increase of roughing cutting speed v_1, the β phase content on the finishing surface increased at first and then decreased obviously, and the maximum value of β phase appeared at the cutting speed of 160 m/min (15.4%). However, the β phase content reached the minimum value when the cutting speed v_1 of rough machining was 80 m/min. Because the finishing parameters were fixed, the phase distribution of finishing surface was directly affected by roughing cutting speed. However, there was no obvious difference between the rapid unloading temperature of workpieces and the rapid cooling stage of cooling to room temperature in the whole seven groups of experiments, so it was inferred that with the increase of roughing cutting speed v_1, the work hardening of the surface to be machined in finishing firstly increased and then decreased. The transformation from α phase to β phase in finishing

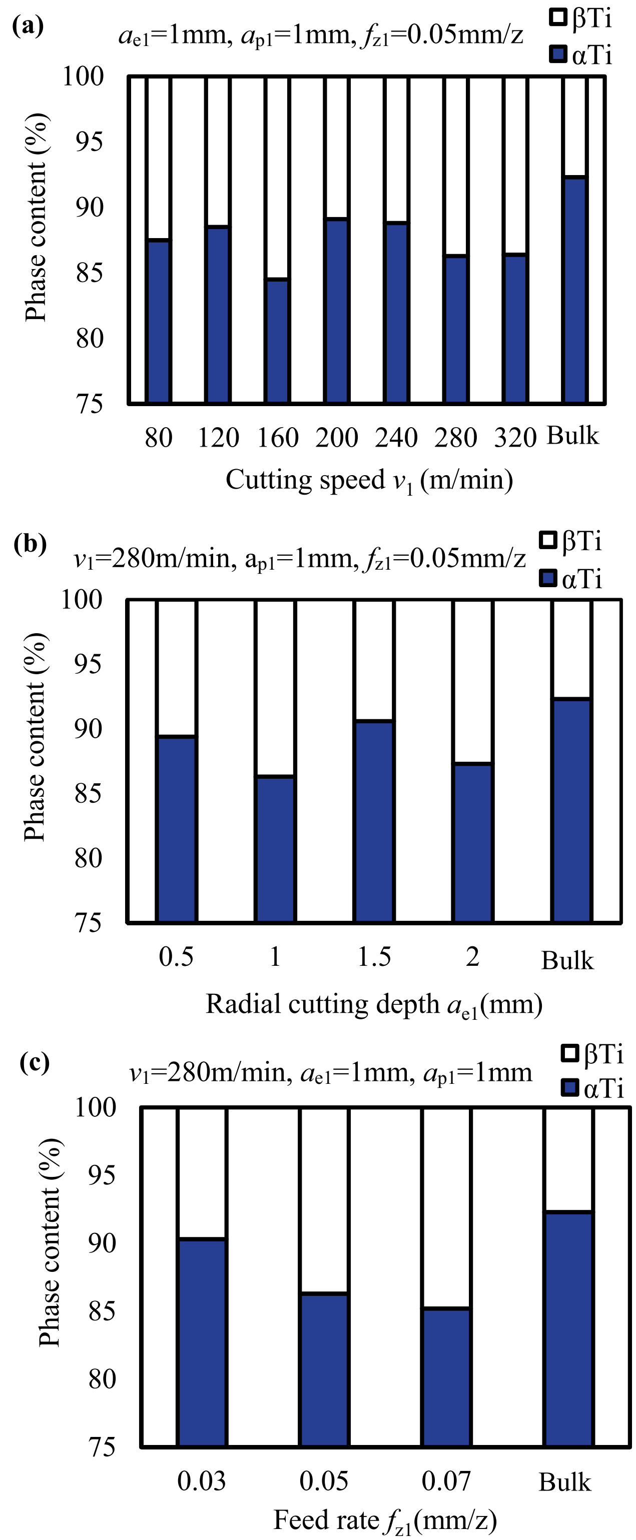

Fig. 12 Effect of cutting parameters on phase content of Ti-6Al-4V alloy machined surface (**a**) cutting speed v_1, (**b**) radial cutting depth a_{e1}, and (**c**) feed rate f_{z1}

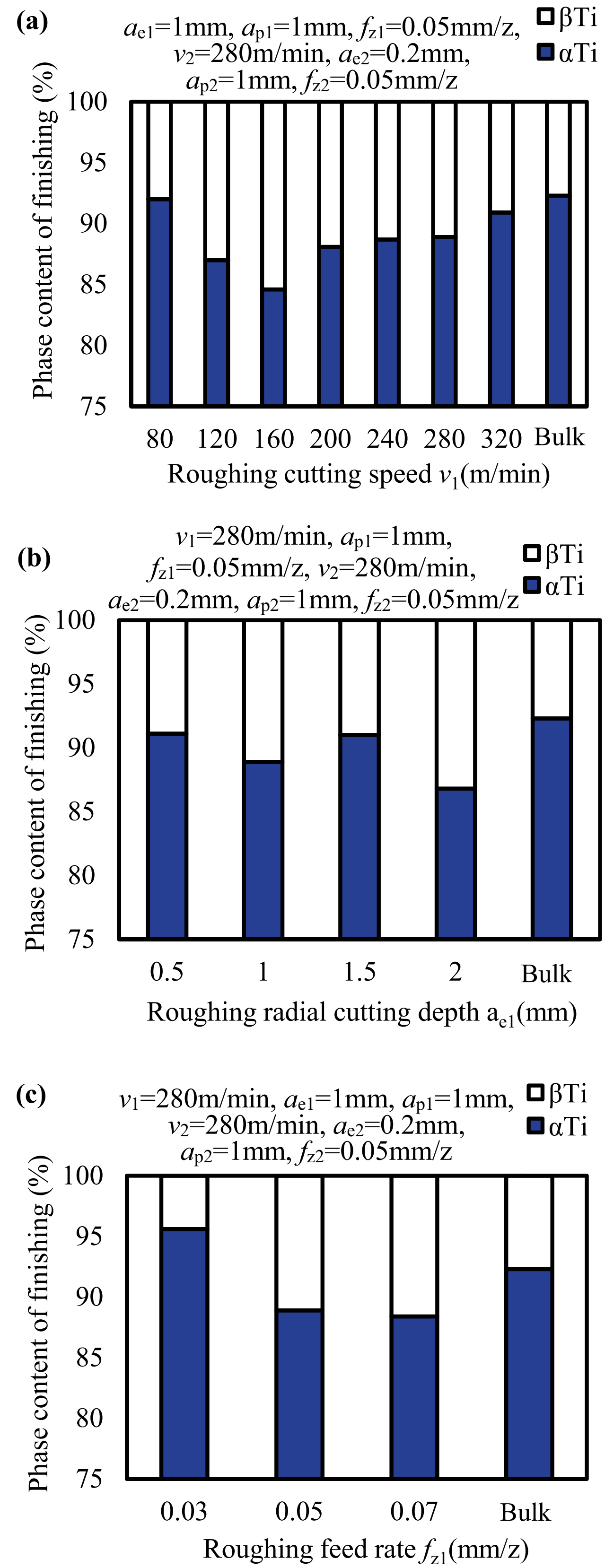

Fig. 13 Effect of roughing cutting parameters on phase content of Ti-6Al-4V alloy machined surface of finishing (**a**) cutting speed v_1, (**b**) radial cutting depth a_{e1}, and (**c**) feed rate f_{z1}

firstly increases and then decreases, which was reflected in the phase transformation trend as shown in Fig. 13a.

It can be seen from Fig. 13b that as the radial cutting depth ae1 increased, the proportion of α and β phases did not change visibly, which indicated that the radial cutting depth ae1 of roughing had no obvious effect on the distribution of phase content on the finishing surface. It can be seen from Fig. 13c that with the increase of feed rate f_{z1} in roughing, the β phase content on the finishing surface gradually increased, which was the same as the trend appearing on the surface in single-step machining. When f_{z1} was 0.07 mm/z, the β phase content on the finishing surface reached the maximum value of 11.6%.

3.5 Crystallite size of machined surface layer

Grain is often used to characterize the morphological characteristics of materials, and its size is called grain size. In the cutting process of Ti-6A1-4V, the severe mechanical load and thermal load make the grain size change [41]. At present, the calculation of cutting grain size of titanium alloy is mostly based on the captured pictures of microstructure by super wide-depth-of-field microscope or scanning electron microscope, and then calculating the average grain size by professional software such as Image Pro. According to the diffraction peak data obtained by XRD, the variation of crystallite size in multi-step cutting of titanium alloy was calculated and analyzed by using the Scherrer equation.

The crystallite size calculated according to Eq. (2) is shown in Fig. 14. The average crystallite size of Ti-6Al-4V bulk material was 28.26 nm. It can be seen from Fig. 14a that the crystallite size of the machined surface was obviously smaller than that of the bulk material surface, which indicated that the machined surface had obvious grain refinement.

In the single-step cutting process, with the cutting speeds increase to the range between 80 and 240 m/min, the crystallite size increased as a whole, and its value varied from the minimum 17.53 to the maximum 24.40 nm. The crystallite size fluctuated slightly near the maximum value with the cutting speed varying from 240 to 320 m/min. When the cutting speed was within the range of 80 to 120 m/min, the cutting force firstly increased and then decreased. After the cutting speed reached 120 m/min, the cutting force basically showed a downward trend. The plastic deformation of the machined surface weakened, and the cutting temperature increased with the increase of cutting speed. The refinement of crystallites weakened and the crystallite size grew. On the other hand, when the cutting speed was greater than 200 m/min, the cutting force did not decrease obviously.

With the increase of cutting speed, although the total heat was higher, the heat introduced into the workpiece increased slightly, which was not enough to produce

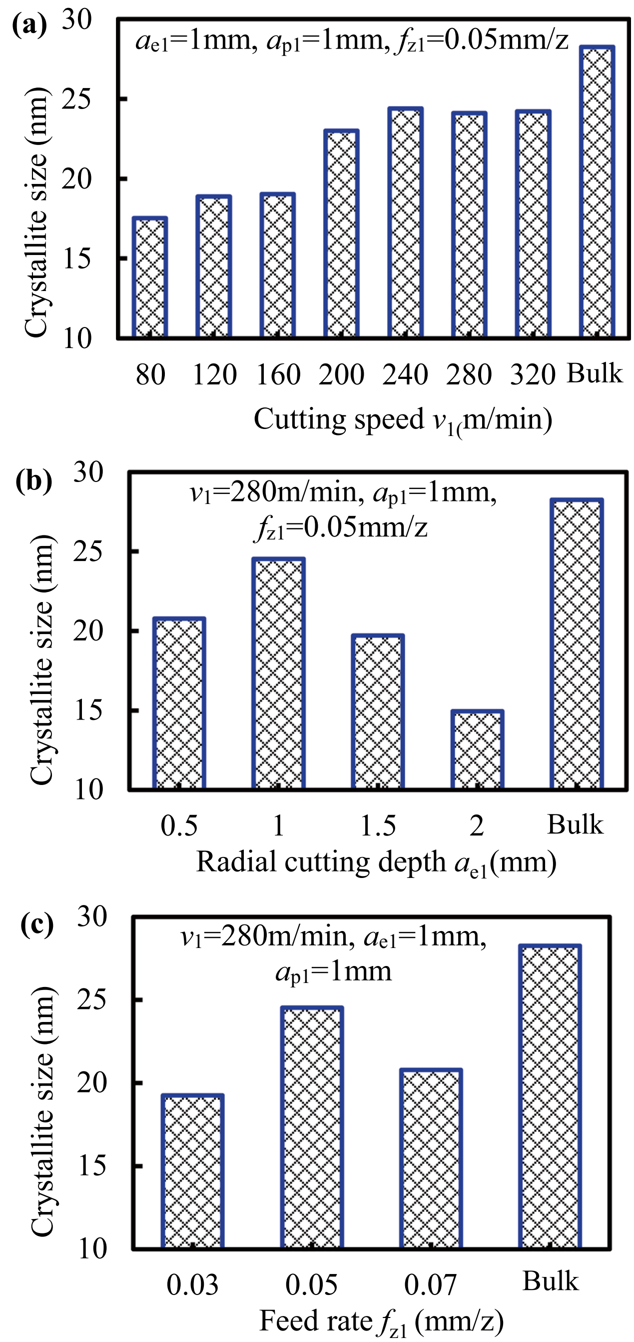

Fig. 14 Effect of cutting parameters on crystallite size of Ti-6Al-4V alloy machined surface (**a**) cutting speed v_1, (**b**) radial cutting depth a_{e1}, and (**c**) feed rate f_{z1}

obvious crystallite growth on the machined surface. It explained the phenomenon that the crystallite refinement did not weaken synchronously when the cutting speed increased in the range of 240 to 320 m/min. The relationship between crystallite refinement and cutting force and cutting temperature showed that at the microcrystal level, the macro micron grain refinement rule in the cutting process still followed, that was, with the increase of plastic deformation, the grain elongated and broke, and the grain refinement strengthened. However, with the increase of cutting temperature, the grain refinement weakened.

It can be seen from Fig. 14b that with the increase of radial cutting depth, the crystallite size on the machined surface firstly increased and then decreased, which were all smaller than the crystallite size of the bulk material. The maximum crystallite size was 24.54 nm at the radial cutting depth of 1 mm, and the minimum crystallite size was 14.96 nm at the radial cutting depth of 2 mm. From the previous conclusions, it can be concluded that as the radial cutting depth increased, the cutting force increased, and the plastic deformation of the corresponding machined surface increased, which promoted the refinement of crystallites. At the same time, the increase of radial cutting depth also led to the increase of cutting temperature and inhibited the refinement of crystallites. The size of crystallite was determined by their combined action. When the radial cutting depth increased from 0.5 to 1 mm, the cutting force increased little. The enhancement of plastic deformation promoted crystallite refinement less than the inhibition caused by the increase of temperature. However, compared with the variation of cutting temperature, the main cutting force increased more obviously, and the plastic deformation increased significantly with the radial cutting depth varying from 1 to 2 mm. Therefore, the crystallite refinement was significantly enhanced so that the crystallite size was the smallest at the radial cutting depth of 2 mm.

As shown in Fig. 14c, with the increase of feed rate, the crystallite size increases slightly at first and then decreases, and the variation of crystallite size is much smaller than that caused by the change of cutting speed and radial cutting depth. According to the analysis of the previous results, the cutting force increased with the increase of feed rate, and the plastic deformation was enhanced, which promoted the crystallite refinement. On the other hand, the cutting temperature also increased with the increase of feed rate, which inhibited the crystallite refinement. Both cutting force and cutting temperature did not increase in direct proportion with the increase of feed rate. The refinement degree of crystallites was determined by plastic deformation and cutting temperature.

Figure 15a shows the influence of roughing cutting speed on the crystallite size of finishing surface. With roughing cutting speed increasing to the range between 80 and 240 m/min, the crystallite size of finishing surface had no obvious change trend, but under the conditions of roughing cutting speed of 280 m/min and 320 m/min, the crystallite size of finishing surface was obviously larger than that at lower cutting speed. Meanwhile, the crystallite refinement of the finishing surface was the weakest.

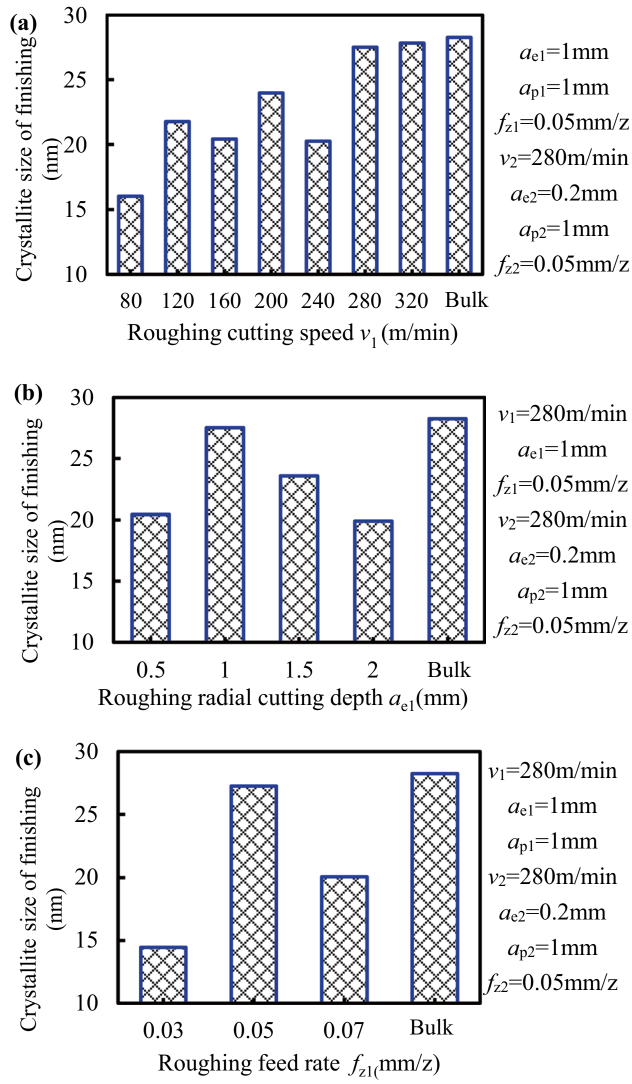

Fig. 15 Effect of roughing cutting parameters on crystallite size of Ti-6Al-4V alloy machined surface of finishing (**a**) cutting speed v_1, (**b**) radial cutting depth a_{e1}, and (**c**) feed rate f_{z1}

The analysis of the relationship between single-step cutting parameters and crystallite size showed that crystallite size was affected by plastic deformation and cutting heat. According to the analysis of experimental results, under the condition of low roughing cutting speed, severe work hardening enhanced the plastic deformation during finishing cutting, which made the crystallites refine seriously, and led to the increase of cutting force and residual compressive stress. Under the condition of high roughing cutting speed, the work hardening effect weakened, which made the microcrystallization of the machined surface weaken and the cutting force decrease. It was beneficial to improve the surface quality of finish machining. However, the reduction of compressive residual stress on the finishing surface reduced the service life of the workpiece.

Figure 15b shows the variation trend of crystallite size on finishing surface under the condition of different roughing radial cutting depths. The microcrystal size increased first and then decreased, and the trend was the same as rough machining. The maximum crystallite size was 27.25 nm at the radial cutting depth of 1 mm, and the minimum crystallite size was 19.90 nm at the radial cutting depth of 2 mm. The crystallite refinement at the radial cutting depth of 2 mm was obvious. The larger radial cutting depth of rough machining had a more significant effect on machining surface hardening, which made the plastic deformation of finishing surface significantly increase and the crystallite size significantly decrease. Figure 15c reveals the influence of the feed rate in roughing on the crystallite size on the finishing surface. With the increase of feed rate in roughing, the crystallite size on the finishing surface increased at first and then decreased. The crystallite size was the smallest under the condition of low roughing feed rate (0.03 mm/z), which showed that this roughing parameter had the most significant influence on the plastic strain of finishing surface.

4 Conclusions

Through the two-step milling cutting experiment of titanium alloy, the influence of rough machining parameters on the cutting force of roughing and finishing and the residual stress of finishing surface was studied by fixing the finish machining parameters and changing the cutting speed, radial cutting depth, and feed rate of roughing, respectively. Furthermore, the microstructure of the machined surface of two-step machining was studied, and the change mechanism of microstructure of roughing and finishing surface under different rough machining parameters was revealed. The conclusions are as follows:

1. The cutting force of finishing changed obviously under the influence of rough machining. Compared with the feed rate and radial cutting depth, the cutting speed in rough machining had the most significant effect on the cutting force in finishing. The finishing cutting force increased with the increase of cutting speed at low roughing cutting speed, and reached the maximum cutting force at 160 m/min. Under the condition of higher cutting speed, the cutting force basically showed a decreasing trend.
2. The results of residual stress detection showed that compressive residual stress existed on the finishing surface. Compared with other cutting parameters, cutting speed had a more significant effect on residual stress. The residual stress reached the maximum in the low-speed cutting range (80 m/min, 120 m/min), and then with the increase of roughing cutting speed, the residual compressive stress increased at first and then decreased. The larger compressive residual stress occurred at the lower radial cutting depth and feed rate of rough machining.
3. With the change of machining parameters, the peak intensity and width of each XRD diffraction pattern changed, and they were all larger than the peak intensity and width of the bulk material. It indicated that the crystallinity of the machined surface was improved, and the influence of microcrystal refinement and slip occurred. In the two-step machining process, the change of roughing cutting speed had the greatest influence on the β phase distribution of finishing surface and the radial cutting depth was smallest. The β phase content on the finishing surface firstly increased and then decreased as the roughing cutting speed increased.
4. According to the analysis of the results, with the increase of cutting speed, the crystallite size of finishing surface increased, and kept larger size at higher cutting speed. However, with the increase of roughing cutting radial depth and feed rate, the crystallite size of finishing surface decreased first and then increased. It can be concluded that the high roughing cutting speed weakened the crystallite refinement phenomenon of finishing surface. With the increase of roughing cutting speed, the work hardening effect weakened, at this time, the crystallite refinement of the machined surface weakened, and the cutting force decreased, which was beneficial to improve the quality of finished surface.

Author contribution Conceptualization, R.Z. and A.L.; methodology, R.Z., A.L., and X.S.; software, R.Z., and X.S.; validation, R.Z., A.L., and X.S.; formal analysis, R.Z. and A.L.; investigation, R.Z., A.L., and X.S.; data curation, R.Z. and X.S.; writing—original draft preparation, R.Z. and X.S.; writing—review and editing, R.Z., X.S., and A.L.; visualization, R.Z. and X.S.; supervision, A.L.; project administration, A.L.; funding acquisition, A.L. All authors have read and agreed to the published version of the manuscript.

Funding The authors would like to acknowledge the financial support of the Natural Science Foundation of Shandong Province (ZR202102210134), the National Natural Science Foundation of China (51605260), the Key Research and Development Program of Shandong Province (2019JZZY010114), and the Young Scholars Program of Shandong University (2018WLJH57).

Availability of data and material The datasets generated and analyzed during the current study are available from the corresponding author on reasonable request.

Declarations

Ethics approval Not applicable.

Consent to participate The authors declared their approval to participate in the submitted manuscript.

Consent for publication The authors declare that they all agree to publish this manuscript.

Conflicts of interest The authors declare no competing interests.

References

1. Ezugwu EO (2005) Key improvements in the machining of difficult-to-cut aerospace super alloys. Int J Mach Tools Manuf 45(12):1353–1367
2. Niinomi M (2003) Recent research and development in titanium alloys for biomedical applications and healthcare goods. Sci Technol Adv Mater 4:445–454
3. Pervaiz S, Rashid A, Deiab I, Nicolescu M (2014) Influence of tool materials on machinability of titanium and nickel-based alloys: a review. Mater Manuf Process 29(3):219–252
4. Hong H, Riga AT, Cahoon JM (1993) Machinability of steels and titanium alloys under lubrication. Wear 162:34–39
5. Dai S, Zhu Y, Huang Z (2016) Microstructure evolution and strengthening mechanisms of pure titanium with nano-structured surface obtained by high energy shot peening. Vacuum 125:215–221
6. Leskovar P, Ferlan D, Kovac M (1987) Residual stresses as essential criteria for the evaluation of production processed. Ann CIRP 36:409–412
7. Ulutan D, Ozel T (2011) Machining induced surface integrity in titanium and nickel alloys: a review. Int J Mach Tools Manuf 51(3):250–280
8. Ginting A, Nouari M (2009) Surface integrity of dry machined titanium alloys. Int J Mach Tools Manuf 49:325–332
9. Hou GM, Li AH (2021) Effect of surface micro-hardness change in multi-step machining on friction and wear characteristics of titanium alloy. Appl Sci 11(16):7471
10. Bermingham MJ, Kirsch J, Sun S, Palanisamy S, Dargusch MS (2011) New observations on tool life, cutting forces and chip morphology in cryogenic machining Ti-6Al-4V. Int J Mach Tools Manuf 51(6):500–511
11. Song X, Li A, Lv M, Lv H, Zhao J (2019) Finite element simulation study on pre-stress multi-step cutting of Ti-6Al-4V titanium alloy. Int J Adv Manuf Technol 104(5–8):2761–2771
12. Choi Y (2017) Influence of rake angle on surface integrity and fatigue performance of machined surfaces. Int J Fatigue 94:81–88
13. Sun H, Li AH, Zhou YH, Song XH, Xue CY (2020) Surface integrity enhancement of aluminum-silicon piston alloy ZL109 employing the forward and reverse finish cutting method. Int J Adv Manuf Technol 107(1–2):617–629
14. Hou GM, Li AH, Song XH, Sun H, Zhao J (2018) Effect of cutting parameters on surface quality in multi-step turning of Ti-6Al-4V titanium alloy. Int J Adv Manuf Technol 98(5–8):1355–1365
15. Abboud E, Attia H, Shi B, Damir A, Thomson V, Mebrahtu Y (2016) Residual stresses and surface integrity of Ti-alloys during finish turning-guidelines for compressive residual stresses. Procedia CIRP 45:55–58
16. Sun J, Guo YB (2009) A comprehensive experimental study on surface integrity by end milling Ti–6Al–4V. J Mater Process Technol 209(8):4036–4042
17. Sridhar BR, Devananda G, Ramachandra K (2003) Effect of machining parameters and heat treatment on the residual stress distribution in titanium alloy IMI-834. J Mater Process Technol 139(1):628–634
18. Dehmani H, Salvatore F, Hamdi H (2013) Numerical study of residual stress induced by multi-steps orthogonal cutting. Procedia CIRP 8:299–304
19. Zlatin N, Field M (1973) Procedures and precautions in machining titanium alloys. In: Jaffee RI, Burte HM (eds) Titanium science and technology. Springer, Boston, MA, USA, pp 489–504
20. Sasahara H, Obikawa T, Shirakashi T (1996) FEM analysis of cutting sequence effect on mechanical characteristics in machined layer. J Mater Process Technol 62(4):448–453
21. Donachie MJ (2000) Titanium: a technical guide. ASM International
22. Wang QQ, Liu ZQ, Wang B (2017) Stress-induced orientation relationship variation for phase transformation of a-Ti to β-Ti during high speed machining Ti-6A1-4V. Mater Sci Eng A 690:32–36
23. Huang Y (1991) A user-material subroutine incorporating single crystal plasticity in the ABAQUS finite element program. Harvard University, Massachusetts
24. Wang QQ, Liu ZQ (2017) Investigation the effect of strain history on crystallographic texture evolution based on the perspective of macro deformation for high speed machining Ti-6A1-4V. Mater Character 131:331–338
25. Li AH, Pang JM, Zhao J (2017) FEM-simulation of machining induced surface plastic deformation and microstructural texture evolution of Ti-6A1-4V alloy. Int J Mech Sci 123:214–223
26. Wang QQ, Liu ZQ, Yang D (2017) Metallurgical-based prediction of stress-temperature induced rapid heating and cooling phase transformations for high speed machining Ti-6Al-4V alloy. Mate Des 119:208–218
27. Pan Z, Liang SY, Garmestani H (2019) Finite element simulation of residual stress in machining of Ti-6Al-4V with a microstructural consideration. Proc Inst Mech Eng Part B: J Eng Manuf 233(4):1103–1111
28. Masmiati N, Sarhan AAD, Hassan MAN, Hamdi M (2016) Optimization of cutting conditions for minimum residual stress, cutting force and surface roughness in end milling of S50C medium carbon steel. Measurement 86:253–265
29. Hauk V (1997) Structural and residual stress analysis by nondestructive methods. Elsevier Science, Danvers, MA
30. Snoha J (1996) X-ray diffraction characterization of process-induced residual stress. Army Research Laboratory ARL-TR-1204
31. Fitzpatrick ME, Fry AT, Holdway P, Kandil FA, Shackleton J, Suominen L (2002) Determination of residual stresses by X-ray diffraction. Meas Good Practice Guide 52:1–59
32. Wang D, Fan Q, Shi R, Zhou Y (2020) In-situ investigation via high energy X-ray diffraction of stress-induced (0002) α→ (110) β transformation in a Ti-5.5Mo-7.2Al-4.5Zr-2.6Sn-2.1Cr alloy. Mater Sci Eng A 779:139–154
33. Dehmani H, Salvatore F, Hamdi H (2013) Multistep hybrid approach applied to material removal operation using cutting tool. 21st French Congress of Mechanics, August 26–30, Bordeaux, France (FR)
34. Velásquez JDP, Tidu A, Bolle B, Chevrier P, Fundenberger JJ (2010) Sub-surface and surface analysis of high speed machined Ti–6Al–4V alloy. Mater Sci Eng A 527(10–11):2572–2578
35. Bai J, Bai Q, Tong Z (2018) Theoretical model for subsurface microstructure prediction in micro-machining Ti-6A1-4V alloy Experimental validation. Int J Mech Sci 148:64–72
36. Williams JC, Baggerly RG, Paton NE (2002) Deformation behavior of HCP Ti-AI alloy single crystals. Metall Mater Trans A 33(3):837–850
37. Leyens C, Peters M (2003) Titanium and titanium alloys: fundamentals and applications. John Wiley & Sons

38. Ducato A, Fratini L, Micari F (2014) Prediction of phase transformation of Ti-6A1-4V titanium alloy during hot-forging processes using a numerical model. Proc Inst Mech Eng Part L J Mat Des Appl 228(3):154–159
39. Ahmed T, Rack HJ (1998) Phase transformations during cooling in α+β titanium alloys. Mater Sci Eng A 243(1–2):206–210
40. Esmaily M, Mortazavi SN, Todehfalah P (2013) Microstructural characterization and formation of a' martensite phase in Ti-6Al-4V alloy butt joints produced by friction stir and gas tungsten arc welding processes. Mater Des 47:143–150
41. Li A, Pang J, Zhao J (2019) Crystallographic texture evolution and tribological behavior of machined surface layer in orthogonal cutting of Ti-6Al-4V alloy. J Mater Res Technol 8(5):4598–4611